Particle agglomeration study in rf silane plasmas: *In situ* study by polarization-sensitive laser light scattering

C. Courteille,[a] Ch. Hollenstein, J.-L. Dorier, P. Gay, W. Schwarzenbach, and A. A. Howling
Centre de Recherches en Physique des Plasmas, Ecole Polytechnique Fédérale de Lausanne, PPB-Ecublens, CH-1015 Lausanne, Switzerland

E. Bertran and G. Viera
Deparatament de Fisica Aplicada I Electronica, Universitat de Barcelona, Av. Diagonal 647 E-08028 Barcelona, Spain

R. Martins and A. Macarico
FCTUNL/Materials Science Department P-2825 Monte de Caparica, Portugal

(Received 18 March 1996; accepted for publication 17 May 1996)

To determine self-consistently the time evolution of particle size and their number density *in situ* multi-angle polarization-sensitive laser light scattering was used. Cross-polarization intensities (incident and scattered light intensities with opposite polarization) measured at 135° and *ex situ* transmission electronic microscopy analysis demonstrate the existence of nonspherical agglomerates during the early phase of agglomeration. Later in the particle time development both techniques reveal spherical particles again. The presence of strong cross-polarization intensities is accompanied by low-frequency instabilities detected on the scattered light intensities and plasma emission. It is found that the particle radius and particle number density during the agglomeration phase can be well described by the Brownian free molecule coagulation model. Application of this neutral particle coagulation model is justified by calculation of the particle charge whereby it is shown that particles of a few tens of nanometer can be considered as neutral under our experimental conditions. The measured particle dispersion can be well described by a Brownian free molecule coagulation model including a log-normal particle size distribution. © *1996 American Institute of Physics.* [S0021-8979(96)07616-5]

I. INTRODUCTION

Particles generated *in situ* during plasma-enhanced chemical vapor deposition (PECVD) or plasma etching can pose serious problems in microelectronic fabrication as the contamination of a wafer surface.[1,2] Furthermore, under certain conditions low-pressure rf discharge can be such prodigious particle generators that they may have commercial potential for the production of ceramic powders.[3,4] In either circumstance, the lack of understanding as to the mechanism of particle synthesis in plasmas is a severe handicap to process optimization and quality control.

Considerable theoretical effort has been made to understand phenomena such as particle charging,[5–7] particle transport,[8] their coupling,[9] particle forces,[10] and their interaction with the plasma.[11–13] Experimentally, in most cases, the particles are detected either *in situ* by laser light scattering[1–3,14–21] or measured by *ex situ* by transmission electron microscopy (TEM).[14,15] However, at present it might be concluded that a lack of quantitative *in situ* measurements of size and number density particles persists.[1,10,17]

The aim of this work is to experimentally study the particle agglomeration. The first part of the article is dedicated to the description of the plasma reactor and the choice of the plasma and diagnostic parameters. To determine the time development of the particle size and the particle number density, three angle polarization-sensitive light scattering was used. The theory and procedure employed for this will be described in the first part. The multi-angle scattering method allowed to determine self-consistently the time development of the particle radius R_p and particle number density N_p provided that the Mie theory is applicable. Data analysis and results of our experiments are given in the second part. We will show that the presence of a cross-polarization intensity in the scattered light excludes the application of the Mie theory during a certain time interval since it indicates the presence of nonspherical particles. TEM measurements will be used to demonstrate the existence of nonspherical particles and to determine the particle size distribution. In this part, we will present some interpretations that can be done from obtained results in particular on the agglomeration phenomena. The third part of this article will be devoted to modeling of the agglomeration by Brownian free molecule coagulation, commonly used in aerosol physics. Using a simple model based first of all on the equality of electron and ion currents and also on the plasma charge neutrality, we calculated the time development of the particle charge and the electron density. We will show that the size dispersion can be well described by a log-normal distribution.

II. EXPERIMENTAL DESCRIPTION

A. Experimental arrangement

The reactor was designed specifically to study particle formation in dusty plasmas. The rf capacitive reactor (Fig. 1) has two cylindrical stainless-steel electrodes of 130 mm di-

[a]Electronic mail: courteil@crppsun3.epfl.ch

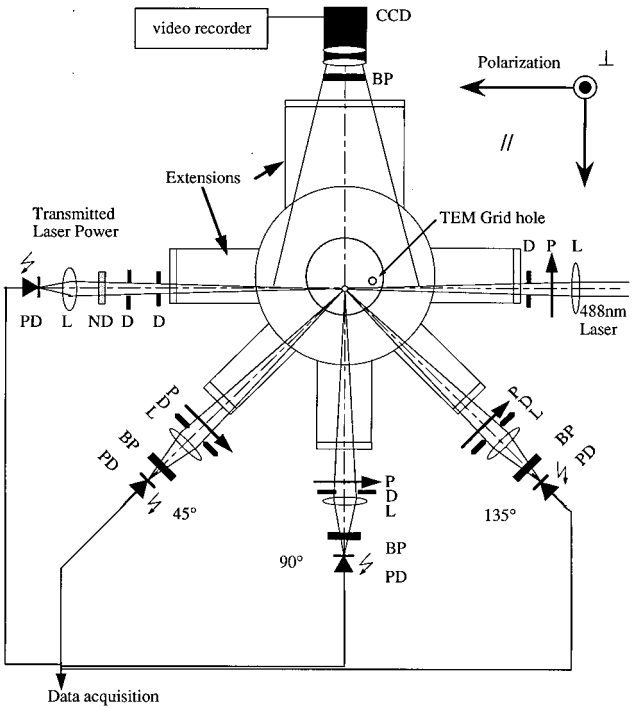

FIG. 1. Schematic top view of the experimental arrangement, showing the plasma reactor, the laser beam transmission measurement, and the three angle detection of the laser beam scattering. The laser-powder interaction path measured by a CCD camera is also shown. P:polarizer, L:lens, D:Diaphragm, BP:488 nm bandpass filter, ND:neutral density filter, PD:photodetector.

ameter, with an electrode gap of 26 mm. The cylindrical vacuum vessel of 360 mm diameter has six radial ports for scattering diagnostics at (0°, 45°, 90°, 135°, 180°, and 270°). The upper rf electrode is surrounded by a concentric grounded guard ring, isolated with polytetrafluorothylene (PTFE), to avoid plasma excitation along its lateral surface. It is capacitively coupled via a π-matching box and a power meter to a wideband rf amplifier driven by a function generator. A passive rf voltage probe, directly connected to the rf electrode, measures the rf and the dc self-bias voltage. The effective power dissipated in the plasma is estimated using the subtractive method.[22,23] The rf electrode holds a gas shower head composed of 168 holes of 1 mm diameter uniformly distributed over the surface. A second gas inlet is positioned at the reactor wall with a diffusor in front to reduce powder perturbation by gas drag. The stainless-steel grounded electrode is equipped with a rotating powder collector for TEM analysis. Twelve TEM grids can successively be exposed to the plasma during a certain time, through a 3 mm hole positioned 43 mm off electrode axis. The pumping consists of a throttle valve, a roots pump, and a primary pump. The throttle valve is controlled by a pressure control feedback system measured by a capacitive gauge.

For the polarization-sensitive light scattering measurements, extension tubes were installed at each aperture to avoid deposition on the windows. Stress free quartz windows are used to avoid depolarization of the polarized laser beam. As a light source, a variable power argon ion laser beam (488 nm) was used. It is focused to obtain a beam waist diameter of 1 mm. A polarizer selects the source polarization either parallel ($\parallel$) or perpendicular ($\perp$) to the scattering plane. After crossing the reactor and a neutral density (ND) filter, the transmitted signal is focused onto a silicon photodiode. Two diaphragms, in front of the neutral density filter, are used to suppress the contribution of the forward scattering. The measurement of this transmitted signal is also used to equalize the two incident polarization intensities before measurements and to check the reproducibility of the powder development. The multi-angle laser light scattering diagnostic consists of three identical independent detection systems composed of a polarizer, a diaphragm to define the solid angle (4.5×10^{-4} sr), a collection lens, a bandpass filter, and a linearly calibrated silicon photodiode. The intersection of the laser beam and the solid angle of the detector defines the scattering volume of 1 mm^3. The three scattered signals and the transmitted intensity are simultaneously digitized by an acquisition system. An additional large window allows the use of a charge coupled device (CCD) camera in order to determine the laser-powder interaction path during the powder time development. The four photodiode signals were measured from plasma ignition in four different laser and detector polarization combinations ($\parallel\parallel$, $\perp\perp$, $\parallel\perp$, $\perp\parallel$, by convention the first symbol is the polarization of the incident beam, $\parallel$ means a polarization in the scattering plane).

B. Plasma parameters

To study powder formation, it is necessary to find optimal plasma parameter conditions for a stable and reproducible powder time development. To avoid misinterpretation of the measurements, an extensive study was devoted to find the gas flow and plasma conditions to assure a homogeneous powder development over large parts of the discharge volume. The incident beam and the detectors can be moved to any axial point within the electrode gap and radially by ±40 mm, due to the limitations of the window width at 45° and 135°. In addition, the scattering volume was placed where powder production is not influenced by powder transport from outside. The experimental parameters chosen were an excitation frequency of 13.56 MHz at a plasma power of 2.9 W. The reactor was maintained at ambient temperature to give high powder yield, minimizing at the same time the temperature gradients thus avoiding an additional complexity of powder dynamics induced by thermophoretic forces.[24] All the reported experiments here were made in pure Silane plasmas. To achieve homogeneous powder development both gas inlets were used with a total silane flow rate of 7.7 sccm and a pressure maintained at 0.25 mbar. The laser was positioned 5 mm above the grounded electrode and 29 mm off electrode axis towards the detectors.

A supplementary study was devoted to the laser fluence-powder interaction which, it was found, could also lead to misinterpretation of the measurements. High laser power can possibly influence the particle development by heating, evaporation, thermophoresis effects, or photodetachment.[1,25–27] Figure 2 represents the evolution of the normalized transmitted intensity (T/T_0) for various laser fluences in the plasma. As can be seen, below 7.5 W/cm^2, the

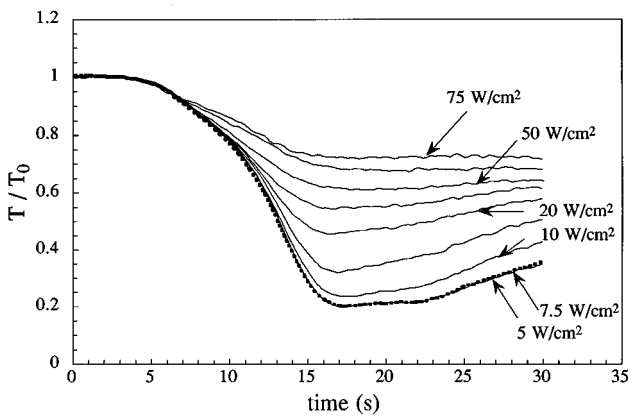

FIG. 2. Time evolution of the normalized transmitted intensity of the laser beam T/T_0 for different incident laser fluences at the plasma. Plasma ignition at time=0 s. Plasma parameters: 7.7 sccm silane at 0.25 mbar, rf plasma power 2.9 W at 13.56 MHz, reactor and electrodes at room temperature. Ar^+ laser at 488 nm wavelength, positioned 5 mm above the lower electrode and displaced by 29 mm towards the detectors from the electrode axis.

laser power does not influence the transmitted intensity; above this value, the laser light influences the particle formation within the laser path. Two explanations can describe this phenomena, evaporation of the particles by the laser beam and/or the thermophoretic effect caused by a temperature gradient between the laser path and the rest of the plasma. All the following time development experiments were done with a laser fluence of 5 W/cm^2.

C. Theory

Elastic light scattering by spherical homogeneous particles is described by the Rayleigh–Gans theory for particles smaller than about $R_p<0.1\lambda$, and by the Lorenz–Mie theory[28,29] for larger particles. The iterative procedure to obtain the time evolution of the radius and the density of particles using the single angle light scattering measurements at 90° is described in Ref. 30. The linear polarization degree, $P=(W_{\perp\perp}-W_{\parallel\parallel})/(W_{\perp\perp}+W_{\parallel\parallel})$ which depends on the refractive index $m=m_r+im_i$, is independent of the particle number density but is a multivalued function of the size parameter x $(x=2\pi R_p/\lambda)$. To solve the indetermination problem of four unknown quantities (R_p, N_p, m_r, m_i) from three independent measurements ($W_{\perp\perp}$, $W_{\parallel\parallel}$, and T/T_0), the scattering angular dissymmetry method can be used. To our knowledge, this technique is rarely used for powder formation studies, except for Selwyn *et al.*[18] and Schmidt *et al.*,[31] who measure the scattered light at 90° and 12°. For our measurements of the scattered intensities at three angles (45°, 90°, and 135°), we used the same iterative method as applied for one angle to determine the time development of the radius and the number density of particle. For each value of m_r and m_i, the BHMIE algorithm[28] calculates the three values of the linear polarization degree and the scattered intensities, which have to simultaneously fit the corresponding experimental points.

For very small particle (Rayleigh) scattering, the expression for the scattered intensity, for the perpendicular polarization and for a number particle density N_p in a detection volume ΔV with a solid angle $\Delta\Omega$, is isotropic and is given by[28]

$$W_{\perp}=C_{\text{scatt}}\cdot I_0\cdot\frac{\Delta\Omega}{4\cdot\pi}\cdot N_p\cdot\Delta V, \tag{1}$$

where I_0 is the incident laser power in W/m^2 and C_{scatt} the scattering cross section defined, for small particles, as

$$C_{\text{scatt}}=\frac{128\cdot\pi^5\cdot R_p^6}{3\cdot\lambda^4}\cdot\left|\frac{m^2-1}{m^2+2}\right|^2. \tag{2}$$

For the parallel polarization $W_{\parallel\parallel}$, the scattered intensity is always zero at 90°, giving a simple experimental criterion for the validity of the Rayleigh approximation. Assuming monodisperse particles all along the laser path, the transmitted power fraction, T/T_0, is independent of the polarization

$$\frac{T}{T_0}=\exp[-C_{\text{ext}}\cdot N_p\cdot d], \tag{3}$$

where d is the laser path length. C_{ext} is the line-averaged extinction cross section (sum of the scattering and absorption cross sections, where the first one is negligible for refractive index typical for amorphous silicon).

$$C_{\text{ext}}=C_{\text{scatt}}+c_{\text{abs}}\approx C_{\text{abs}}=\frac{8\cdot\pi^2\cdot R_p^3}{\lambda}\cdot\text{Im}\left\{\frac{m^2-1}{m^2+2}\right\}. \tag{4}$$

The laser path length d was evaluated from measurements with the CCD camera. This measurement is important to accurately determine the particle number density. The ratio between Eq. (1) and the logarithm of Eq. (3) leads to the relative particle radius. The necessary calibration to obtain absolute N_p and R_p values was done from TEM measurements. For this reason, particles for TEM measurements are collected at the Rayleigh–Mie transition time, coinciding with the appearance of the $W_{\parallel\parallel}$ intensity, to calibrate the scattered light intensity. This calibration allowed to determine the absolute particle size and the deduction of the number particle density as a function of the discharge time.

III. RESULTS

During the powder development, we successively measured scattered signals with each of the four different polarization configurations $\parallel\parallel$, $\perp\perp$, $\perp\parallel$, $\parallel\perp$ at three angles during four consecutive reproducible plasma runs. For each measurement the transmitted signal was used to check the discharge and powder reproducibility. From the appearance of the $W_{\parallel\parallel}$ intensity at 90° we determine the Rayleigh–Mie transition time: $t_{\text{R-M}}=6$ s. For $t<t_{\text{R-M}}$ we apply the Rayleigh theory, for $t>t_{\text{R-M}}$ we use the Mie theory. In this latter region, from the multiangle scattering signals, we determine the polarization degree P at 45°, 90°, and 145°, from which we estimate the particle radius development.[32] Figure 3(a) represents the time development of P for the three angles; the signals are reproducible down to the smallest details. In Fig. 3(b), the cross-polarization intensity at 135° normalized to the corresponding direct polarization $W_{\perp\parallel}/W_{\perp\perp}$ ($W_{\parallel\perp}/W_{\parallel\parallel}$ shows similar behavior) is presented. The angle 135° was chosen since, according to Mie theory[28,33] the cross-

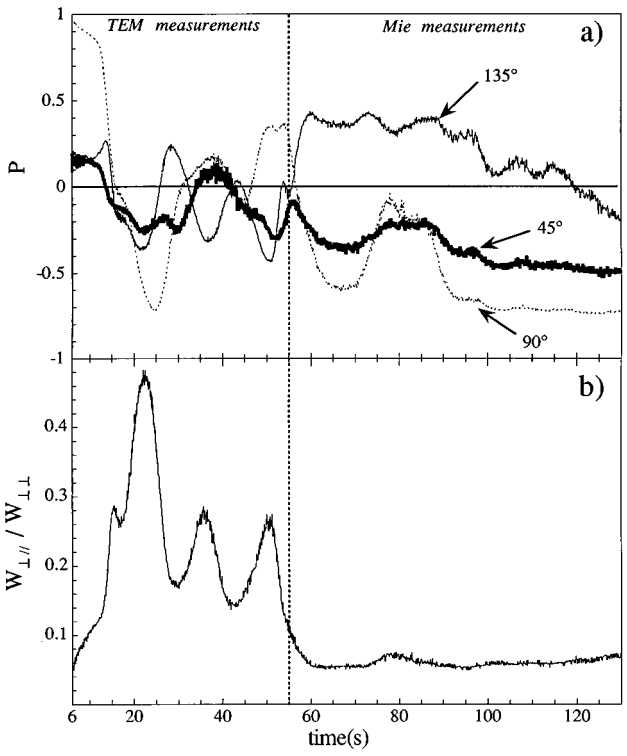

FIG. 3. Time development of (a) the linear polarization degree, P, at 45°, 90°, and 135°, and (b) of the cross-polarization intensity normalized to the corresponding direct polarization $W_{\perp\parallel}/W_{\perp\perp}$ at 135°. Plasma parameters and laser position as for Fig. 2, with a laser intensity of 5 W/cm^2.

polarization intensity is predicted to be larger for angles near to back scattering. The appearance of the cross-polarization signal indicates nonspherical particles and/or multiple scattering. Placing the detectors just above the laser path allowed to estimate the multiple-scattering contribution which did not exceed 5%–10% of the direct polarization intensity. It can therefore be concluded that nonspherical particles are present within the scattering volume if the cross-polarization signal exceeds this limit. Consequently we can distinguish two different regimes following the Rayleigh phase: The first one, between roughly 7 and 55 s, where $W_{\perp\parallel}/W_{\perp\perp}$ is significantly above the multiple-scattering contribution, indicates the presence of nonspherical agglomerates; the second, for times larger than roughly 55 s, where only negligible cross-polarization intensities are detected, indicating that again spherical particles exist. This fact is confirmed by TEM analysis of particle deposition on two subsequent independent runs showing a good reproducibility. The advantage of the polarization-sensitive laser light scattering with respect to circular polarization methods[21] is the sensitivity to the cross-polarization intensity. Therefore the assumption and the degree of sphericity of the particles can be checked *in situ*. Additional information about the particle geometry may be obtained by more sophisticated scattering theories. This is, however, out of the scope of the present article. Micrographs presented in Fig. 4 show collected particles or agglomerates which are suspended in the plasma for different discharge times. For these experiments, TEM grids are exposed during a period of 4 s, exposure starting 1 s before the plasma extinction. The first picture, Fig. 4(a) shows small spherical particles of about 40 nm in radius collected after 6 s of plasma. This result was used to calibrate the particle sizes and the particle number densities at the Rayleigh–Mie transition region. Fig. 4(b) shows that nonspherical agglomerates are collected after 15 s of plasma. For this time the cross polarization ratio $W_{\perp\parallel}/W_{\perp\perp}$ is approximately 30%. Figures 4(c) and 4(c) are representative for particles collected 77 s after plasma ignition, Fig. (d) being an enlargement of Fig. (c). All the clusters collected are again nearly spherical, showing a blackberrylike structure. The constituents of these structures are of the order of a few tens of nm diameter and form a densely packed nearly spherical-like structure. Strictly speaking, the original Mie theory[34] does not apply to nonspherical particles and therefore the Mie theory in its original form is not applicable in the time interval between 7 and 55 s. Recovering of spherical geometry of the particles later in the development allows again the application of the Mie scattering theory and therefore the determination without ambiguity of R_p and N_p. Within the interval (7 and 55 s), we have used the TEM micrographs to measure the particle size. The Rayleigh theory is used to obtain the R_p and N_p evolution up until a discharge time of 6 s. The present size detection limit for our experimental arrangement is estimated to be in the order of about 2 nm radius.

From the plasma physics side we note that large cross-polarization signals are usually accompanied by instabilities with frequencies in the Hz region, visible on the scattered light as well as on the transmitted signal and on the plasma light emission. It could be speculated that these instabilities arise from the local depletion of electron density, as discussed later. These very low-frequency instabilities are often observed in dusty plasmas.[35–38] Figure 5 represents the ratio $W_{\perp\parallel}/W_{\perp\perp}$ with the level of low-frequency noise filtered out of the transmitted signal for plasma parameters slightly different than shown before.

Figure 6 shows the time evolution of the particle radius R_p and the particle number density N_p calculated from Rayleigh theory for 2–6 s into the time development. During this Rayleigh phase two regimes can be distinguished: the first one, from 2 to 2.67 s, in which the particle size grows rapidly at about 27 nm/s, whereas the particle number density drastically decreases. At the beginning of this agglomeration phase particles as small as a few nm are present in the plasma with a particle number density N_p in the order of 10^{16}–10^{17} m^{-3}. This very high density has also been observed in other experiments.[15,21] Within this time period the volume fraction ($\nu_f = 4/3 \cdot \pi \cdot N_p \cdot R_p^3$), presented in the inset, is found to be roughly constant. The second regime, from 2.67 until 6 s, shows a much slower growth rate of about 6.5 nm/s, whereas the particle number density N_p reaches a density in the range of about 10^{15} m^{-3}.

For larger particles, TEM and Mie measurements were used to determine the particle size and the particle number density. For the nonspherical agglomerates we determined from TEM pictures the equivalent radius defined as the radius of a sphere with a volume equivalent to the sum of the volumes of the individual sticking particles in the agglomerate.[39] The TEM analysis shows a broadening of the

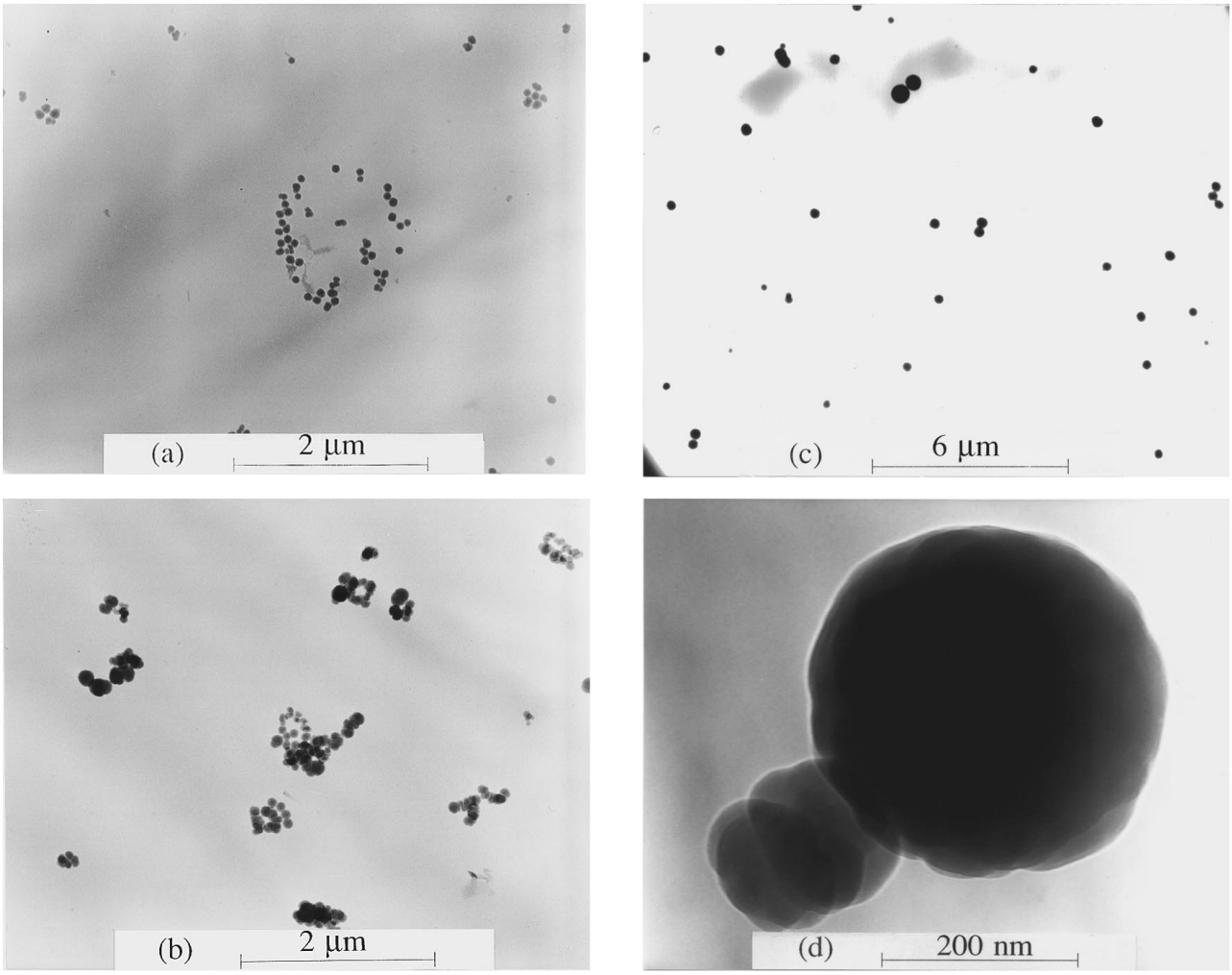

FIG. 4. Micrographs of particles collected after different discharge durations: (a) after 6 s plasma, (b) after 15 s plasma, (c) and (d) after 77 s plasma. (d) is an enlargement of a part of (c). Plasma parameters as for Fig. 2.

particle size distribution during the time development of the particles. After 55 s, the cross-polarization signal became negligible and the Mie theory could be applied. A typical refractive index for high hydrogen content *a*:Si–H material of 3.5–0.3 *i* was taken (in contrast to the value 3–5 *i* used by Shiratani *et al.*[21] for the same wavelength) to determine R_p and N_p, corresponding to the best simultaneous fit to the three polarization degrees and intensities. We now attribute the previous high values for the refractive index,[30] in the early stages of particle development, to an artifact due to the erroneous application of the Mie theory to nonspherical particles, as revealed by the cross-polarization intensity. Figure 7 represents the time evolution of R_p and N_p determined, in chronological order, by the Rayleigh theory, TEM measurements, and the Mie theory. In the last region, we have also added the size dispersion obtained from TEM analysis.

IV. DISCUSSION

A. Coagulation model

In aerosol physics, agglomeration phenomena can, in certain cases, be described by Brownian free molecular coagulation (BFMC) in the regime $K_n > 10$ (where K_n is the Knudsen number defined as $K_n = \lambda / R_p$, where λ is the mean free path of gas molecules).[39–41] In order to describe the agglomeration in the Rayleigh phase, between 2 and 2.67 s, we have used the BFMC model where particles collide as a result of their Brownian motion. In this simplified model forces such as the van der Waals attractive force, the Coulomb repulsive force, and the laminar shear effect are not taken into account. In this model agglomeration starts from a given radius R_c and a given number density of particles N_c. According to the BFMC model the time development of the radius and the number density of particles is given by[41]

$$\frac{N_p}{N_c} = (1 + C \cdot K \cdot b \cdot \nu_g^{1/6} \cdot N_c \cdot t)^{-6/5}, \tag{5}$$

$$\frac{R_p}{R_c} = (1 + C \cdot K \cdot b \cdot \nu_g^{1/6} \cdot N_c \cdot t)^{2/5}, \tag{6}$$

with $C = \frac{5}{6} \cdot (2^{5/12} + 2^{13/12} + 2^{1/60}) = 3.721$, K the collision coefficient defined as: $K = (\frac{3}{4} \cdot \pi)^{1/6} \cdot (6 \cdot k \cdot T / \rho)^{1/2}$ with ρ the particle density and T the temperature (300 K), b a numerical factor which has been shown to approach the asymptotic value of 0.7415, and ν_g the initial particle volume

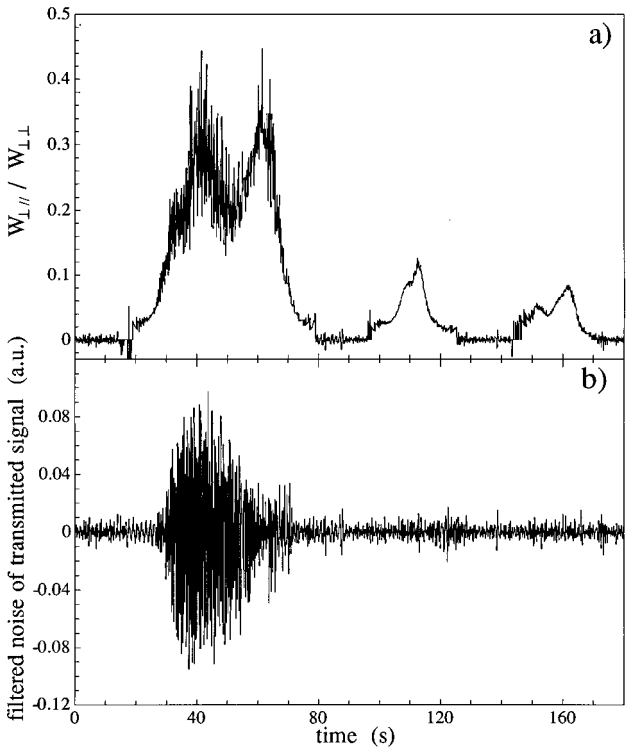

FIG. 5. Time development of (a) the $W_{\perp\parallel}/W_{\perp\perp}$ ratio and (b) the level of the low-frequency noise filtered out of the transmitted signal. Plasma parameters: 15.4 sccm silane at 0.20 mbar, rf power 3.3 W at 13.56 MHz, reactor and electrodes at room temperature.

$(4/3\cdot\pi\cdot R_c^3)$. This model requires two assumptions: first, a constant volume fraction necessary for the determination of R_p and second, charge neutrality of the particles. As far as the first one is concerned, we have already mentioned that the volume fraction $(4/3\cdot\pi\cdot N_p\cdot R_p^3)$ stays constant during the first seconds of the Rayleigh phase. Concerning the neutrality, it is well known[7,42] that dust particles suspended in a plasma acquire a negative charge due to the high electron mobility compared to the positive ion mobility, behaving like floating Langmuir probes. In the following we describe the

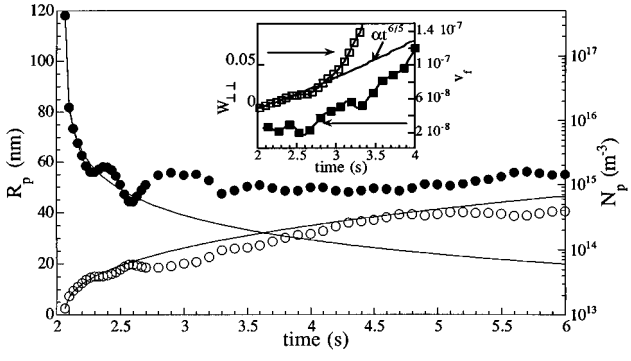

FIG. 6. Time development of the particle radius R_p (○), and the number density N_p (●) for early discharge times (Rayleigh scattering). Solid lines show the best fit of the Brownian free molecule coagulation model (R_c=2.4 nm and $N_c=4\times10^{17}$ m^{-3}) The inset presents the first second of the scattered light time evolution (□) and $t^{6/5}$ time dependence fit and the volume fraction ν_f (■). Plasma parameters and laser position as for Fig. 2.

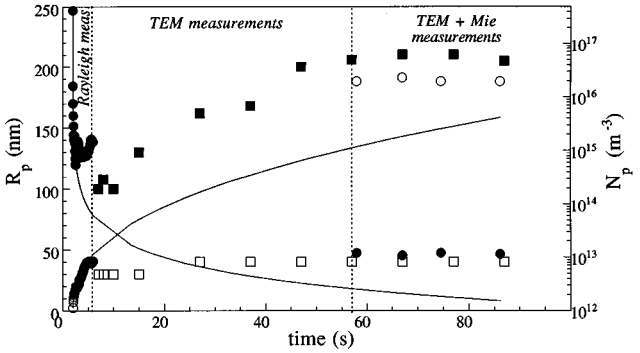

FIG. 7. Time development of the particle radius R_p (○) and the number density N_p (●), and the lower (□) and the upper limit (■) of particle radius obtained from the TEM measurements. Solid lines fit from the Brownian free molecule coagulation model as in Fig. 6. Plasma parameters and laser position as for Fig. 2.

model used to calculate the number of elementary charges Z_p carried by the particle from the experimental values of R_p and N_p and for the BFMC model. Note that, in contrast to negative ions, the particles considered here are large enough to experience charge fluctuations due to statistical variations in electron/ion fluxes to their surface.[43,7] The particle potential adjusts to ensure equality of the electron and positive ion currents: $I_e=I_i$.

The electron current impinging on the particle is[44]

$$I_e=e\cdot n_e\cdot\pi\cdot R_p^2\cdot\sqrt{\frac{kT_e}{m_e}}\cdot\exp\left[\frac{e}{kT_e}\cdot(\phi_p-\phi_0)\right], \tag{7}$$

where ϕ_p and ϕ_0 are the surface potential of the particle and plasma potential, respectively.

Using the orbital motion limit (OML), and assuming the ion thermal velocity larger than the ion drift velocity, the positive ion current to the particles can be written as

$$I_i=e\cdot n_i\cdot\pi\cdot R_p^2\cdot\sqrt{\frac{kT_i}{m_i}}\cdot\left(1-\frac{e}{kT_i}\cdot[\phi_p-\phi_0]\right). \tag{8}$$

Equalizing the electron and the ion currents leads to

$$1-\tau\cdot\Delta=\frac{n_e}{n_i}\cdot\sqrt{\frac{m_i}{m_e}}\cdot\tau\cdot\exp(\Delta), \tag{9}$$

where $\tau=T_e/T_i$, and $\Delta=(e/kT_e)\cdot(\phi_p-\phi_0)$.
The plasma charge neutrality is given by

$$n_e+e\cdot Z_p\cdot N_p=n_i, \tag{10}$$

with Z_p being the number of elementary charges on the particle related to its surface potential,[45] given for spherical particles by

$$Z_p=\frac{C_p}{e}\cdot(\phi_p-\phi_0)=\frac{4\cdot\pi\cdot\epsilon_0}{e}\cdot R_p\cdot(\phi_p-\phi_0), \tag{11}$$

where C_p is the capacitance of a spherical particle.

By normalizing the neutrality equation to the positive ion density, we can obtain

$$n_e/n_i+P'_H\cdot\Delta=1, \tag{12}$$

where $P'_H = 4\cdot\pi\cdot\epsilon_0/e\cdot R_p/n_i\cdot N_p\cdot kT_e$ is the Havnes parameter normalized to n_i instead of n_e as usually used.[44]

In our case the ratio of the electronic and ionic temperatures is about 80. Previous mass spectrometry measurements[30] [Fig. 7(a)] show that the positive ion density can be considered as roughly constant after the appearance of the first small particles. For this reason a normalization to n_i was chosen.

The simultaneous resolution of Eqs. (9), (11), and (12), T_e, T_i, and n_i being taken constant and N_p and R_p being either the experimental data or the theoretical points from the BFMC model, gives an estimation of the time development of the number of elementary charges Z_p on the particles and the ratio n_e/n_i. In this simple model we don't take into account the negative ion density, important in electronegative plasmas, or the secondary electron emission due to ion bombardment which in general tends to modify the value of Z_p. The calculation of the particle charge from the Rayleigh scattering experimental points shows that a particle in this phase of development has a maximum of one charge. Therefore particles of this size undergo strong charge fluctuations[7] ($Z_p/\langle Z_p\rangle = 0.5\cdot|\langle Z_p\rangle|^{-1/2}$) and can be considered on average as neutral particles. Trapped particles larger than $R_p > 190$ nm are charged with more than about 100 e. Therefore, assuming particle neutrality in the early phase of the time development, we can compare our experimental data with the BFMC model. The agglomeration starts, if, for instance, trapped negative ions in the plasma grow to sufficient size of about a few nm. In this case, the particle behavior changes from an ionic to a floating probe behavior.[46] These small particles undergo the above-mentioned charge fluctuations and finally coagulate. From the BFMC model it is deduced that the large particle number density at the beginning of the agglomeration is necessary to obtain particle sizes comparable to the observed one. Trapping of negative ions and/or attachment-detachment cycling[47] are possible mechanisms which may lead, in different works, to the observed high particle densities. Other possible mechanisms, such as fast growth of neutrals, may lead directly to sufficiently sized particles with the necessary high particle density. In our case, the starting radius and starting number density of neutral particles at the beginning of the agglomeration were arbitrarily chosen from the first experimental point in the Rayleigh phase: $R_c = 2.4$ nm and $N_c = 4\times10^{17}$ m^{-3}. The result is represented by a solid line in Fig. 6. On Fig. 6 we can see a very good agreement between the raw data and the theoretical points, between 2 and 2.67 s (other R_c and N_c values giving a less good fit). After 2.67 s there is a discrepancy in the particle number density, whereas the radius time evolution in the Rayleigh phase is still well described by the model. From the BFMC theory it can be shown that the scattered light intensities should follow a $t^{6/5}$ law.[40] The small inset in Fig. 6 represents the scattered light time evolution and a fit to it with a time dependence of $t^{6/5}$. This is again an indication that at least the beginning of the agglomeration phase can be well described by the Brownian free molecule coagulation model. In Fig. 7, the solid lines represent the theoretical time evolution of the radius and particle number density, from BFMC, until the end of the time development. A discrepancy between the prediction of the BFMC and measured sizes and densities obtained by Mie scattering is observed. The difference might be attributed to particle charging slowing down the agglomeration.

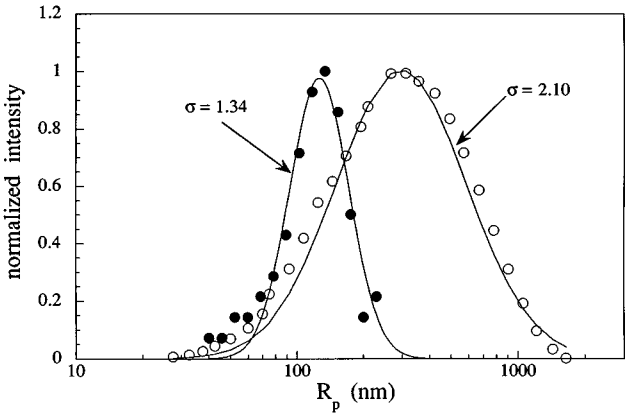

FIG. 8. The log-normal radius distribution of particle radius (○) from TEM samples, for the same plasma parameter as Fig. 2, obtained in steady-state conditions, and (●) from powder collected on the cold lower electrode after several hours of plasma operation (12.3 sccm silane at 0.20 mbar, rf plasma power 2.9 W at 13.56 MHz).

The TEM measurements presented in Fig. 7 indicate a nonmonodisperse particle size distribution during the whole particle formation. Figure 8 shows the particle radius distributions of spherical particulates collected on the TEM grids, in steady-state conditions after 67 s from the plasma ignition, and from powder deposited on the electrode after several hours of dusty plasma for different discharge parameters. For the latter case, the powder sample was diluted in isopropanol and analyzed by dynamic laser light scattering, whereas the particle size on the grids were determined from TEM analysis. These *ex situ* measurements are fitted to log-normal size distributions $A\cdot\exp[-[\ln^2(R_p/R_0)]/[2\cdot\ln^2(\sigma)]]$ in Fig. 8. We can therefore state that the particle radius distribution, in steady-state conditions, can be closely described by a log-normal distribution. For the powder collected on the grid a geometric standard deviation[40,41] of $\sigma = 1.34$ is obtained. The standard deviation for the powder collected on the electrode, under different plasma conditions, was found to be $\sigma = 2.10$.

The basic theory of Brownian coagulation in the free molecular regime was extended by Lee *et al.*[41] for particles with a log-normal size distribution function. This approach assumes that the size distribution attains or can at least be represented by a time-dependent log-normal distribution function all along the coagulation process. From a given initial log-normal distribution the whole time evolution of the distribution function can be calculated. Interestingly, it has been shown that for long times into the coagulation phase the geometric standard deviation approaches $\sigma = 1.35$ independently of its initial value.

Following the work of Lee *et al.*, the time evolution of the log-normal distribution was calculated for the same critical values N_c and R_c as mentioned above. As described in the last section, TEM analysis gives the size dispersion as a function of the discharge time. Figure 9 shows the maximum and minimum particle radius of the TEM measurements

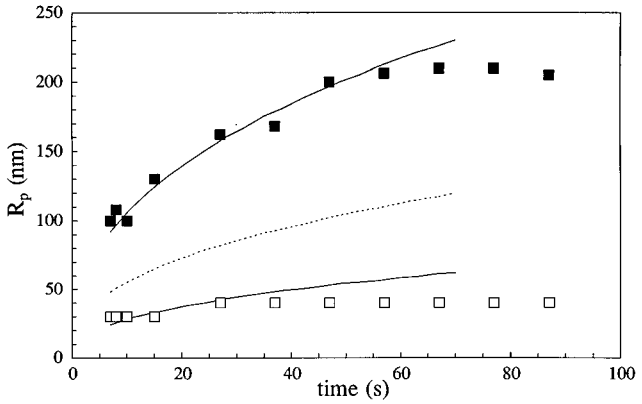

FIG. 9. Comparison between the particle radius distribution measured from the TEM measurements, the lower (□) and the upper limit (■), and calculated from Brownian free molecular coagulation model with self-preserving log-normal distribution. Dashed lines represent the particle radius at the maximum and solid lines at 10% of the maximum of the log-normal distribution.

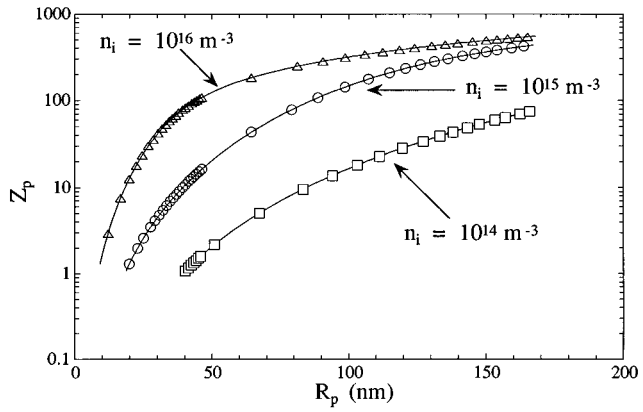

FIG. 10. Calculated number of elementary charges Z_p on the particle as a function of the particle radius, for different positive ion densities n_i.

compared with the calculated radius dispersion from the log-normal distribution. The dashed line corresponds to the radius at the maximum of the distribution and the solid lines represent the particle radius at 10% of its maximum. A reasonably good agreement between the results from the TEM observations and the free molecular coagulation model extended to self-preserving log-normal distribution can be stated. It should be noted that small size particles of about 40 nm remain in the discharge all along the time development, whereas large particles increase in size with time. This observation is similar to recent work by Shiratani *et al.*[21] However, we can rule out in our conditions any formation of new particle generations or bimodal-like particle size distributions similar to the ones reported by Shiratani *et al.* No experimental evidence for a gap in the particle size distribution was found. Two possible explanations for this discrepancy can be considered. The first one concerns the differences in the powder formation in pure and (highly) diluted plasmas,[21] which might be shown by the fact that the nature of the diluting gas influences the powder localization[48] and even the powder time development. We observed that argon dilution advances, whereas helium dilution tends to retard the powder appearance time for the same plasma power with respect to pure silane plasmas.[49] Formation of successive generations of particles has, to our knowledge, only been reported in diluted plasmas.[26] Depletion effects in these highly diluted silane plasmas might be responsible for the new particle generation or to bimodal-like particle size distributions. The second explanation may be attributed to the particle counting method from the TEM micrographs with nonspherical agglomerates. Indeed, if each of the small particles constituting an agglomerate is counted separately instead of considering the nonspherical cluster as a single particle with a radius calculated from the sum of the volume of individual sticking particles in the agglomerate, this will lead to a bimodal size distribution. In our case, the presence of the cross-polarization intensity proves that the nonspherical agglomerates do exist in the plasma, must be counted as such, and are not formed only after plasma extinction.

All the various observations presented up until now indicate that the particle agglomeration phase might well be described, within experimental error, by the Brownian free molecular coagulation model. In the frame of this model the particles are assumed to be neutral. Using the above set of Eqs. (9), (11), and (12) the time-averaged particle charge as a function of the particle size was calculated for different ion densities and the results are presented in Fig. 10. Depending on the ion density, particles up to roughly 40 nm can be considered on average to be neutral for low n_i. The agglomeration phase, in particular the initial large increase in the particle size, can therefore be modeled by a neutral coagulation scheme such as Brownian free molecular coagulation. Later in time, increased particle charge might contribute to reduce the agglomeration rate. This effect may explain why, for later times in Fig. 7, the particle number density as given by the BFMC model underestimates the experimental values.

In addition to the particle charge, the electron density can be estimated from the solution of Eqs. (9) and (12). The time dependence of the particle charge and the electron density, corresponding to the best fit of the Brownian free molecular coagulation theory to the experimental results, is presented in Fig. 11. Figure 11 shows again that during the initial agglomeration phase the participating particles can be considered on the average as neutrals. The electron density abruptly decreases during this part of the particle development, followed by an increase which depends on the fixed ion density n_i. For low n_i, the electron density stays approximately at the level reached after the initial agglomeration phase. The drastic decrease of the electron density during the coagulation phase can be understood as follows: The sum of the charges on the very small particles is in detriment of the electron density. Despite the small number of charges per particle, the high particle number density at this early stage of the agglomeration (of the order of 10^{16}–10^{17} m^{-3}) leads to a large consumption of total charge and consequently to a decrease in the electron density. Therefore, even if there are only few charges per particle or charge fluctuations of each particle, their large number density leads to a decrease of the electron density.[50] Larger particles, on the other hand, allow higher charging but their low particle number density limits the number of charges taken from the elec-

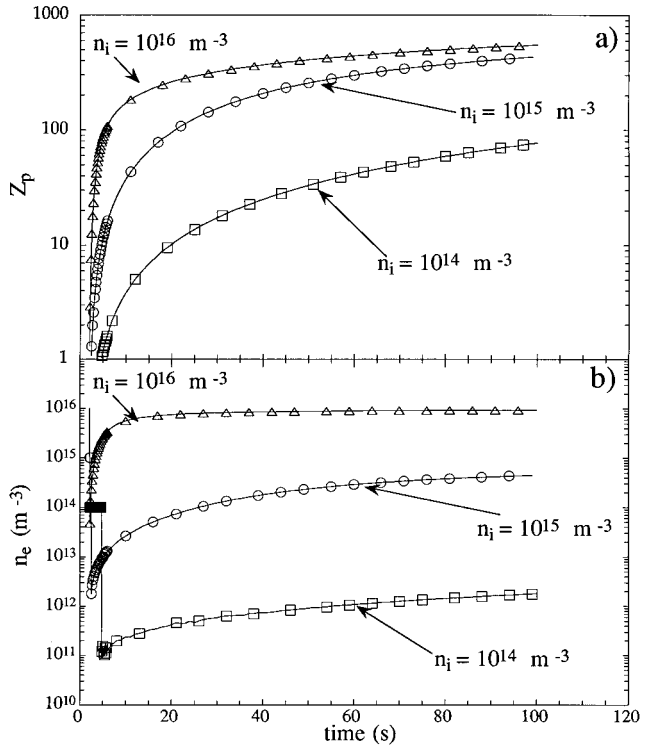

FIG. 11. Calculated time development of (a) the number of elementary charges Z_p on the particle and (b) of the electron density, for different positive ion densities n_i.

tron density. The charges on the large particles only influence the electron density considerably for low values of n_i, since then the number of charges localized on these large particles becomes comparable to the ion density. According to this, we can say that agglomeration ''saves'' the plasma from extinction by decreasing the net total charge on the particles.

V. CONCLUSION

Multi-angle polarization-sensitive laser light scattering has been shown to be a useful diagnostic to determine the time development of the radius and number particle density in low power rf silane plasmas. In contrast to other laser scattering methods it also gives additional information on the sphericity of the dust particles, a necessary information for the comprehension of agglomeration processes and for future applications of plasma produced nanoparticles.

Presence of cross-polarization intensities and *ex situ* TEM measurements showed that during a time interval of the agglomeration phase, nonspherical particles exist. The presence of nonspherical particles restricts the applicability of the original Mie scattering theory. Later in the time development, nearly spherical particles can be found again. The high cross-polarization intensities are accompanied by low-frequency instabilities visible on different plasma diagnostics.

The agglomeration phase has been modeled by a neutral agglomeration scheme, the Brownian free molecular coagulation model (BFMC). Despite the simplicity of the model a good qualitative agreement between the measured particle size and particle number density can be stated. From the BFMC theory extended by a simple model based on the equality of the electron and ion currents and on the plasma charge neutrality the time development of the particle charge and of the electron density normalized to the positive ion density was calculated. It is demonstrated that, for low positive ion densities, particles as large as 40 nm in radius can be considered as neutrals. Therefore particles in the order of up to a few tens of nanometers behave under our conditions like neutrals, at least at the beginning of the coagulation phase. Therefore neutral coagulation schemes can be applied to describe at least the initial step of the increase in particle size. More sophisticated neutral coagulation schemes, including increasing charging of the particles with time and coagulation between charged and uncharged particles, may be necessary to understand in detail the physics of the agglomeration in dusty plasmas. The modeling of the agglomeration phase also allowed to calculate the time behavior of the electron density. The large particle number density of very small particles is responsible for a drastic decrease of the electron density in spite of the low number of charges attributed to each particle. Larger particles, with higher charging, are found to influence the electron density only if the charges occupied by the particles become comparable to the background ion density.

The particle size distribution observed by TEM analysis can be well described by a log-normal distribution. Also, good agreement between the time evolution of the observed size distribution and the particle size distribution, obtained by the BFMC model, including self-preserving log-normal distribution, was found.

ACKNOWLEDGMENTS

The authors thank M. Yanyan Qiu from the FCTUNL for his help in transmission electron microscopy. This work was funded by Swiss Federal Research Grant No. EF-REN(93)035 and No. BBW93.0136 for BRITE/EURAM project No. BE-7328).

[1] K. G. Spears, T. J. Robinson, and R. M. Roth, IEEE Trans. Plasma Sci. **14**, 179 (1986).
[2] G. S. Selwyn, J. Singh, and R. S. Bennett, J. Vac. Sci. Technol. A **7**, 2758 (1989).
[3] P. Ho, S. Buss, and R. E. Loehmann, J. Mater. Res. **4**, 973 (1989).
[4] H. Anderson, T. T. Kodas, and D. M. Smith, Ceram. Bull. **68**, 996 (1989).
[5] A. Barkan, N. D'Angelo, and R. L. Merlino, Phys. Rev. Lett. **73**, 3093 (1994).
[6] D. Winski and M. E. Jones, IEEE Trans. Plasma Sci. **23**, 188 (1995).
[7] J. Goree, Plasma Sources Sci. Technol. **3**, 400 (1994).
[8] M. S. Barnes, J. H. Keller, J. C. Forster, J. A. O'Neill, and D. K. Kushner, Phys. Rev. Lett. **68**, 313 (1992).
[9] H. Ikesi, Phys. Fluids **29**, 1764 (1986).
[10] J. E. Daugherty and D. B. Graves, J. Appl. Phys. **78**, 2279 (1995).
[11] J.-P. Boeuf, Phys. Rev. A **46**, 7910 (1992).
[12] S. J. Choi, P. L. G. Venzek, R. J. Hoekstra, and M. J. Kushner, Plasma Sources Sci. Technol. **3**, 418 (1994).
[13] J.-P. Boeuf, P. Belenguer, and T. Hbid, Plasma Sources Sci. Technol. **3**, 407 (1994).
[14] A. Bouchoule, A. Plain, L. Boufendi, J.-P. Blondeau, and C. Laure, Appl. Phys. **70**, 1991 (1991).
[15] L. Boufendi, A. Plain, J.-P. Blondeau, A. Bouchoule, C. Laure, and M. Toogood, Appl. Phys. Lett. **60**, 169 (1992).

[16] G. M. Jellum and D. B. Graves, Appl. Phys. Lett. **57**, 2077 (1990).
[17] G. M. Jellum and D. B. Graves, J. Appl. Phys. **67**, 6490 (1990).
[18] G. S. Selwyn, J. E. Heidenreich, and K. L. Haller, J. Vac. Sci. Technol. A **9**, 2817 (1991).
[19] G. S. Selwyn, J. E. Heindenreich, and K. L. Haller, Appl. Phys. Lett. **57**, 1876 (1990).
[20] R. M. Roth, K. G. Spears, G. D. Stein, and G. Wong, Appl. Phys. Lett. **46**, 253 (1985).
[21] M. Shiratani, H. Kawasaki, T. Fukuzawa, T. Yoshioka, Y. Ueda, S. Singh, and Y. Watanabe, J. Appl. Phys. **79**, 104 (1996).
[22] C. M. Horwitz, J. Vac. Sci. Technol. A **1**, 1795 (1983).
[23] A. A. Howling, J.-L. Dorier, C. Hollenstein, U. Kroll, and F. Finger, J. Vac. Sci. Technol. A **10**, 1080 (1992).
[24] G. M. Jellum, J. E. Daugherty, and D. B. Graves, J. Appl. Phys. **69**, 6923 (1991).
[25] E. Stoffels and W. W. Stoffels, Ph.D. thesis, Eindhoven, University of Technology, The Netherlands, 1994.
[26] L. Boufendi and A. Bouchoule, Plasma Sources Sci. Technol. **3**, 262 (1994).
[27] R. L. Armstrong, in *Optical Effects Associated with Small Particles*, edited by P. W. Barber and R. K. Chang (Singapore, 1988).
[28] C. F. Bohren and D. R. Huffmann, *Absorption and Scattering of Light by Small Particles* (Wiley, New York, 1983).
[29] H. C. V. d. Hulst, *Light Scattering by Small Particles* (Wiley, New York, 1975).
[30] C. Hollenstein, J.-L. Dorier, J. Dutta, L. Sansonnens, and A. A. Howling, Plasma Sources Sci. Technol. **3**, 278 (1994).
[31] U. I. Schmidt and D. B. Graves, J. Vac. Sci. Technol. A **14**, 595 (1996).
[32] J.-L. Dorier, C. Hollenstein, and A. A. Howling, J. Vac. Sci. Technol. A **13**, 918 (1995).
[33] W. Heller and M. Nakagaki, J. Chem. Phys. **61**, 3619 (1974).
[34] G. Mie, Ann. Phys. **25**, 377 (1908).
[35] A. G. Sitenko, A. G. Zagorodny, and V. N. Tsytovich (to be published).
[36] D. P. Resendes, R. Bingham, and V. N. Tsytovich (to be published).
[37] N. D'Angelo, J. Phys. D **28**, 1009 (1995).
[38] O. Havnes, F. Li, F. Melandso, T. Aslaksen, T. W. Hartquist, G. E. Morfill, T. Nitter, and V. Tsytovich, J. Vac. Sci. Technol. A **14**, 525 (1996).
[39] G. Prado and J. Lahaye, J. Chim. Phys. **4**, 483 (1975).
[40] S. K. Friedlander, *Smoke, Dust and Haze, Fundamentals of Aerosol Behavior* (Wiley, New York, 1977).
[41] K. W. Lee, H. Chen, and J. A. Gieseke, Aerosol Sci. Technol. **3**, 53 (1984).
[42] C. Böhm and J. Perrin, J. Phys. D **24**, 865 (1991).
[43] A. Garscadden, Plasma Sources Sci. Technol **3**, 239 (1994).
[44] O. Havnes, C. K. Goertz, G. E. Morfill, E. Grün, and W. Ip, J. Geophys. Res. **92**, 2281 (1987).
[45] E. C. Whipple, T. G. Northrop, and D. A. Mendis, J. Geophys. Res. **90**, 7405 (1985).
[46] A. C. Breslin and K. G. Emeleus, Int. J. Electron. **31**, 189 (1971).
[47] S. J. Choi and M. J. Kushner, J. Appl. Phys. **74**, 853 (1993).
[48] J.-L. Dorier, Ch. Hollenstein, A. A. Howling, C. Courteille, W. Schwarzenbach, A. Merad, and J.-P. Boeuf, IEEE Trans. Plasma Sci. **24**, 101 (1996).
[49] C. Courteille, L. Sansonnens, J. Dutta, J.-L. Dorier, Ch. Hollenstein, A. A. Howling, and U. Kroll, Proc. 12th European Photovoltaic Solar Energy Conf., Amsterdam, 1994, p. 319.
[50] E. Stoffels, W. W. Stoffels, G. M. W. Kroesen, and F. J. d. Hoog, J. Vac. Sci. Technol. A **14**, 556 (1996).